PHYSICAL REVIEW D **85,** 043016 (2012)

CMB lensing reconstruction in real space

Martin Bucher,[1,2,3] Carla Sofia Carvalho,[4,5,6] Kavilan Moodley,[3,6] and Mathieu Remazeilles[1,2]

[1]*Laboratoire APC, Université Paris Diderot, Bâtiment Condorcet, 10 rue Alice Domon et Léonie Duquet, 75205 Paris Cedex 13, France*

[2]*Laboratoire de Physique Théorique, Bâtiment 210, Université Paris-Sud, 91405 Orsay Cedex, France*

[3]*National Institute for Theoretical Physics (NITheP), Private Bag X54001, Durban 4000, South Africa*

[4]*Intituto de Plasmas e Fusão Nuclear, Instituto Superior Técnico, Av. Rovisco Pais 1, 1049-001 Lisbon, Portugal*

[5]*Research Center for Astronomy and Applied Mathematics, Academy of Athens, Soranou Efessiou 4, 11 527 Athens, Greece*

[6]*Astrophysics and Cosmology Research Unit, University of KwaZulu-Natal, Westville, Durban 4000, South Africa*

(Received 20 April 2010; published 29 February 2012)

We explore the reconstruction of the gravitational lensing field of the cosmic microwave background in real space. We show that very little statistical information is lost when estimators of short range on the celestial sphere are used in place of the customary estimators in harmonic space, which are nonlocal and in principle require a simultaneous analysis of the entire sky without any cuts or excisions. Because virtually all the information relevant to lensing reconstruction lies on angular scales close to the resolution scale of the sky map, the gravitational lensing convergence and shear fields (which unlike the deflection field or lensing potential are directly related to the observations in a local manner) may be reconstructed by means of quadratic combinations involving only closely separated pixels. Even though harmonic space provides a more natural context for understanding lensing reconstruction theoretically, the real space methods developed here have the virtue of being faster to implement and are likely to prove useful for analyzing realistic maps containing a galactic cut and possibly numerous small excisions to exclude point sources that cannot be reliably subtracted.

DOI: 10.1103/PhysRevD.85.043016 PACS numbers: 98.70.Vc

I. INTRODUCTION

Recently there has been much discussion of how the intervening clustered matter between the last scattering surface (at $z \approx 1100$) and an observer at the present time distorts the CMB anisotropy by means of gravitational lensing [1–5]. On the level of the two-point correlation function, this effect distorts the TT (temperature-temperature) correlation power spectrum [6] and mixes the EE and BB polarization power spectra as well as distorting them [7–9]. Lensing also introduces non-Gaussianities that manifest themselves in the higher-point correlation functions [10,11]. At the level of the three-point correlation function, to leading order there is no nonzero expectation value if we regard the lensing potential as a random field [12,13]. However, if we consider the CMB lensing potential Φ as fixed, we find that expectation values of the form

$$\langle T(\boldsymbol{\theta})T(\boldsymbol{\theta}')\rangle_{\Phi(\boldsymbol{\theta}'')} - \langle T(\boldsymbol{\theta})T(\boldsymbol{\theta}')\rangle_{\Phi=0} \tag{1}$$

do not vanish, and this property may be exploited to recover or ''reconstruct'' the lensing field using estimators quadratic in T (or in E and B) [14–16]. Here, $\boldsymbol{\theta}$, $\boldsymbol{\theta}'$ and $\boldsymbol{\theta}''$ denote points on the celestial sphere.

Much effort has been devoted to developing an optimal reconstruction of the lensing potential. Hu and Okamoto [17,18] analyzed lensing reconstruction in Fourier space, noting that in the presence of lensing quadratic combinations of the form $T(\ell)T(\ell')$ have an expectation value proportional to $\Phi(\ell - \ell')$, where Φ is the lensing potential. They constructed an unbiased minimum variance combination of such quadratic factors to obtain an estimator of the lensing potential. This approach in harmonic space is optimal when there is full sky coverage, no galactic cut, no bad pixels due to point sources that must be excised, and no need for nonuniform weighting to account for nonuniform instrument noise [19–21]. However, when these conditions are not satisfied, the harmonic approach offers little guidance on how to proceed. Another approach would be to start with the likelihood for a lensed sky map after linearization. In this way, the problem can be reduced to a linear algebra problem, albeit a rather messy one given the large dimensions of the matrices [22,23]. The improvement gained from using an even more optimal maximum likelihood estimator [24] is marginal in the case of temperature data, though the situation is different for polarization data where the higher order corrections to the quadratic estimator present in the maximum likelihood estimator may no longer be negligible [25].

In this paper we adopt a different, real space approach. For lensing reconstruction the bulk of the statistical information lies at very small scales, near the resolution limit of the survey. The fractional statistical information contributed by the long wavelength temperature and polarization anisotropies is negligible. This fact suggests developing an estimator based on a long-wavelength limit in which the effect of the lensing is approximated as a constant linear transformation of the form $(\boldsymbol{\theta} - \boldsymbol{\theta}_0) = \underline{\mathbf{S}}(\boldsymbol{\theta}' - \boldsymbol{\theta}'_0)$, where $\underline{\mathbf{S}}$ is a matrix and the primed and unprimed coordinates refer to the lensed and unlensed sky, respectively. Such an

estimator provides an optimal weak lensing reconstruction in the limit $|\ell'| \to 0$, but is less optimal at large wave numbers.

Our interest lies in considering slightly nonoptimal estimators that have been modified to have a finite range in pixel space so that cuts, excisions of pixels, and nonuniform coverage may be included in a simple way. We believe that such nonideal but more robust local estimators defined in real space may prove superior for confronting the complications inherent in analyzing real data [22,26,27]; a similar approach is taken in [28]. Another advantage of the approach here is that the convergence and pure shear estimators provide separate and essentially independent lensing reconstructions which may be confronted with each other. This feature may prove useful to diagnose spurious signals, which are unlikely to affect the two reconstructions in the same way. Moreover, the presence of two shear components enables one to estimate the noise of the reconstruction through the implied transverse shear field, which is forbidden in weak lensing.

The organization of the paper is as follows. In Sec. II we derive a simple real space estimator that allows us to recover the convergence field $\kappa_0(\boldsymbol{\theta})$ and two components of the pure shear field $\gamma_+(\boldsymbol{\theta})$ and $\gamma_\times(\boldsymbol{\theta})$ by taking the product of the temperature map with an appropriately filtered temperature map. It is shown that the small scale temperature anisotropies, near the resolution limit of the survey, supply the bulk of the exploitable statistical information. In Sec. III, we show how the range of the filter kernel in angular space can be truncated with very little excess variance, or equivalently information loss. The estimators of Sec. II are unbiased and of minimum variance in the long-wavelength limit of the lensing fields. In Sec. IV, we analyze what happens at larger wave numbers for the lensing fields and also indicate when nonlinearity becomes relevant. Section V digresses slightly by showing how lensing reconstruction estimators can be devised based on particular features in the CMB spectrum. Finally, in Sec. VI we present the results of some simulations validating our approach as well as some concluding remarks.

II. A REAL SPACE LENSING ESTIMATOR

In this section, we develop a simple lensing estimator in real space. First, we develop an estimator of the convergence $\kappa_0(\boldsymbol{\theta})$ and the pure shear $\gamma_+(\boldsymbol{\theta})$, $\gamma_\times(\boldsymbol{\theta})$ that is unbiased and of minimum variance in the limit of long wavelength for the lensing field. Then in the following section, we show how to truncate the support of the filter in an optimal way.

Before deriving and implementing the real space estimator, it is useful to consider the relation between the various descriptions of the lensing and the deformation of the anisotropies in real space. It is also useful to consider which angular scales contribute the most statistical weight to the lensing reconstruction. The CMB anisotropy originating from the surface of last scatter is distorted by intervening matter that deforms the photon paths connecting the surface of last scatter to us today. This distortion may be described in three ways: by a lensing potential Φ, by a deflection field $\boldsymbol{\xi} = -\nabla\Phi$, or by the three components of the deformation tensor

$$\underline{\boldsymbol{\kappa}} = \begin{pmatrix} \kappa_0 + \gamma_+ & \gamma_\times \\ \gamma_\times & \kappa_0 - \gamma_+ \end{pmatrix} = \nabla_a \nabla_b \Phi. \tag{2}$$

Here, κ_0 is the convergence, γ_+ and $\gamma_\times$ are the two pure shear components, and we have neglected a rotation in the shear tensor. The lensed temperature map T' is related to the unlensed temperature T according to $T'(\boldsymbol{\theta}') = T(\boldsymbol{\theta} = \boldsymbol{\theta}' - \boldsymbol{\xi})$. In the most general case, the angular position in the unlensed sky $\boldsymbol{\theta}$ is an arbitrary function of the angular position $\boldsymbol{\theta}'$ in the lensed (observed) sky, which we shall denote $\boldsymbol{\theta} = \underline{\mathbf{S}}(\boldsymbol{\theta}')$, but we shall assume that the lensing is weak, meaning that the displacement and its derivative may be regarded as small.

Even if we had simultaneous access to the entire sky, the descriptions using Φ or $\boldsymbol{\xi}$ would suffer from an ambiguity. The scalar potential Φ cannot be distinguished from $\Phi + (constant)$ and the vector field $\boldsymbol{\xi}$ can be measured only up to a constant translation (or more properly a rotation in the presence of sky curvature). This is because if we know only the CMB power spectrum, a patch of sky and its translation necessarily have the same likelihood on account of the isotropy of the underlying stochastic process. Consequently, the absolute translation due to lensing cannot be observed. By contrast, locally the shear and convergence (which are gradients of the translation vector field) are completely well defined.

Let $\underline{\mathbf{S}}$ be a constant symmetric matrix. We define the lensing transformation as follows:

$$T'(\boldsymbol{\theta}') = T(\boldsymbol{\theta} = \underline{\mathbf{S}}\boldsymbol{\theta}'). \tag{3}$$

We define the transform of the temperature map as

$$a(\boldsymbol{\ell}) = \frac{1}{\sqrt{\mathcal{A}}} \int d^2\theta \exp[i\boldsymbol{\ell}\cdot\boldsymbol{\theta}] T(\boldsymbol{\theta}) \tag{4}$$

where $\mathcal{A}$ is the area (solid angle) of the region of integration, so that $c(\ell) = \langle |a(\boldsymbol{\ell})|^2 \rangle$ and

$$\langle T^2(0) \rangle = \int \frac{d^2\ell}{(2\pi)^2} c(\ell). \tag{5}$$

We now compute the power spectrum $c'(\ell)$ of the ensemble of lensed maps T' in terms of $c(\ell)$ for the unlensed maps T. We have

$$\begin{aligned} a'(\boldsymbol{\ell}) &= \frac{1}{\sqrt{\mathcal{A}'}} \int d^2\theta' \exp[i\boldsymbol{\ell}\cdot\boldsymbol{\theta}'] T'(\boldsymbol{\theta}') \\ &= \frac{1}{\sqrt{\mathcal{A}}} \int d^2\theta \left| \frac{\partial(\theta_1', \theta_2')}{\partial(\theta_1, \theta_2)} \right|^{1/2} \exp[i\boldsymbol{\ell}\cdot\underline{\mathbf{S}}^{-1}\boldsymbol{\theta}] T(\boldsymbol{\theta}) \\ &= \det{}^{-1/2}[\underline{\mathbf{S}}] a(\underline{\mathbf{S}}^{-1}\boldsymbol{\ell}) \end{aligned} \tag{6}$$

so that

$$c'(\ell) = \det^{-1}[\underline{\mathbf{S}}]c(\underline{\mathbf{S}}^{-1}\ell) = \det^{-1}[\underline{\mathbf{S}}]c(|\underline{\mathbf{S}}^{-1}\ell|). \quad (7)$$

We now linearize setting

$$\underline{\mathbf{S}} = \underline{I} + \underline{\boldsymbol{\kappa}} = \begin{pmatrix} 1 & 0 \\ 0 & 1 \end{pmatrix} + \begin{pmatrix} \kappa_0 + \gamma_+ & \gamma_\times \\ \gamma_\times & \kappa_0 - \gamma_+ \end{pmatrix}, \quad (8)$$

so that

$$c'(\ell) = c(|\ell|) - \left[\mathrm{tr}(\underline{\boldsymbol{\kappa}})c(|\ell|) + \frac{(\ell\cdot\underline{\boldsymbol{\kappa}}\cdot\ell)}{|\ell|}\left(\frac{dc(\ell)}{d\ell}\right)\right]_{\ell=|\ell|} \quad (9)$$

and

$$\begin{aligned}\delta c(\ell) &= c'(\ell) - c(|\ell|) \\ &= \kappa_0\left[\ell\frac{dc(\ell)}{d\ell} + 2c(\ell)\right] \\ &\quad + (\gamma_+\cos(2\phi) + \gamma_\times\sin(2\phi))\left[\ell\frac{dc(\ell)}{d\ell}\right] \end{aligned} \quad (10)$$

where (ℓ, ϕ) are the polar coordinates of $\boldsymbol{\ell}$. This results in the distorted power spectrum

$$\begin{aligned}c(\ell) \rightarrow c'(\ell) = c(\ell)\times\Bigg[1 &+ \kappa_0\left(\frac{d\ln[c(\ell)]}{d\ln[\ell]} + 2\right) \\ &+ (\gamma_+\cos(2\phi) + \gamma_\times\sin(2\phi))\left(\frac{d\ln[c(\ell)]}{d\ln[\ell]}\right)\Bigg].\end{aligned} \quad (11)$$

This result is not surprising because the derivative $\beta = d\ln c(\ell)/d\ln(\ell)$ is the local spectral index of the power at a given ℓ, with $\beta = -2$ corresponding to a scale-invariant spectrum and $\beta = 0$ corresponding to a white noise spectrum. Thus the spectrum is invariant under pure dilatations (i.e., $\kappa_0 \neq 0$, $\gamma_{+,\times} = 0$) when $\beta = -2$, and is invariant under pure shear transformations (i.e., $\kappa_0 = 0$, $\gamma_{+,\times} \neq 0$) when $\beta = 0$. The distortion of the power spectrum described above mathematically is illustrated in Fig. 1.

In a region of area $\mathcal{A}$ over which κ_0, γ_+, and $\gamma_\times$ are spatially constant, the unbiased minimum variance estimator of κ_0, constructed using inverse variance weighting of the estimators from different ℓ, would be

$$\begin{aligned}\hat{\kappa}_0 = &\frac{1}{\mathcal{A}N_{\hat{\kappa}_0}}\int\frac{\mathcal{A}d^2\ell}{(2\pi)^2}\frac{c(\ell)}{(c(\ell)+n(\ell))^2} \\ &\times\left[\frac{d\ln[c(\ell)]}{d\ln[\ell]} + 2\right](c'_{\mathrm{obs}}(\ell) - \langle c(\ell)\rangle)\end{aligned} \quad (12)$$

where

$$N_{\hat{\kappa}_0} = \int\frac{d^2\ell}{(2\pi)^2}\frac{c^2(\ell)}{(c(\ell)+n(\ell))^2}\left[\frac{d\ln[c(\ell)]}{d\ln[\ell]} + 2\right]^2 \quad (13)$$

where $n(\ell)$ is the instrument noise. In Eq. (12), we subtract a constant bias $\langle c(\ell)\rangle_{\Phi=0}$ because we want to probe the difference with the power spectrum expected in the absence of lensing. The expression for the estimator is obtained in the usual way: using Eq. (11) we make an ansatz for $\hat{\kappa}_0$ that involves an integral over the observed temperature power spectrum with an appropriate weight function and normalization, which are solved for by assuming that the estimator has minimum variance and is unbiased. For a finite region, $\mathcal{A}\int d^2\ell/(2\pi)^2$ corresponds to a discrete sum over modes. Physically, $N_{\hat{\kappa}_0}$ denotes the total $(S/N)^2$ per unit area for a deformation corresponding to $\kappa_0 = 1$.

Setting

$$\begin{aligned}K_{\hat{\kappa}_0}(\theta) &= \frac{1}{N_{\hat{\kappa}_0}}\int\frac{d^2\ell}{(2\pi)^2}\exp[-i\ell\cdot\boldsymbol{\theta}]\frac{c(\ell)}{(c(\ell)+n(\ell))^2} \\ &\quad\times\left[\frac{d\ln[c(\ell)]}{d\ln[\ell]} + 2\right] \\ &= \frac{1}{2\pi N_{\hat{\kappa}_0}}\int_0^\infty \ell d\ell J_0(\ell\theta)\frac{c(\ell)}{(c(\ell)+n(\ell))^2} \\ &\quad\times\left[\frac{d\ln[c(\ell)]}{d\ln[\ell]} + 2\right],\end{aligned} \quad (14)$$

we may rewrite Eq. (12) as

$$\begin{aligned}\hat{\kappa}_0 = &\frac{1}{\mathcal{A}}\int d^2\theta\int d^2\theta' \\ &\times K_{\hat{\kappa}_0}(\theta-\theta')[T(\boldsymbol{\theta})T(\boldsymbol{\theta}') - \langle T(\boldsymbol{\theta})T(\boldsymbol{\theta}')\rangle_{\Phi=0}].\end{aligned} \quad (15)$$

Now the key point is that the kernel $K_{\hat{\kappa}_0}(\theta)$ is peaked at small values of θ, so that we may translate the above localized estimation of κ_0 to different points in the map. Therefore,

$$\hat{\kappa}_0(\boldsymbol{\theta}) = T(\boldsymbol{\theta})(K_{\hat{\kappa}_0}\circ T)(\boldsymbol{\theta}) - \langle T(\boldsymbol{\theta})(K_{\hat{\kappa}_0}\circ T)(\boldsymbol{\theta})\rangle_{\Phi=0}, \quad (16)$$

where the operator $\circ$ denotes a convolution, provides an unbiased minimum variance estimator of the underlying lensing field $\kappa_0(\theta)$ in the long-wavelength limit. The convergence estimator is then simply a product of the observed temperature map with another copy of the temperature map that has been convolved with the kernel, $K_{\hat{\kappa}_0}(\theta)$, with the constant bias removed.

We may analogously estimate the two components of the pure shear as follows:

$$\begin{aligned}\begin{pmatrix}\hat{\gamma}_+ \\ \hat{\gamma}_\times\end{pmatrix} = &\frac{1}{\mathcal{A}N_{\hat{\gamma}_+,\hat{\gamma}_\times}}\int\frac{\mathcal{A}d^2\ell}{(2\pi)^2}\frac{c(\ell)}{(c(\ell)+n(\ell))^2} \\ &\times\left(\frac{d\ln[c(\ell)]}{d\ln[\ell]}\right)\begin{pmatrix}\cos(2\phi) \\ \sin(2\phi)\end{pmatrix}c'_{\mathrm{obs}}(\ell)\end{aligned} \quad (17)$$

where

$$N_{\hat{\gamma}_+,\hat{\gamma}_\times} = \frac{1}{2}\int\frac{d^2\ell}{(2\pi)^2}\frac{c^2(\ell)}{(c(\ell)+n(\ell))^2}\left(\frac{d\ln[c(\ell)]}{d\ln[\ell]}\right)^2 \quad (18)$$

and for the local estimator, again in the long-wavelength approximation, we define the kernel

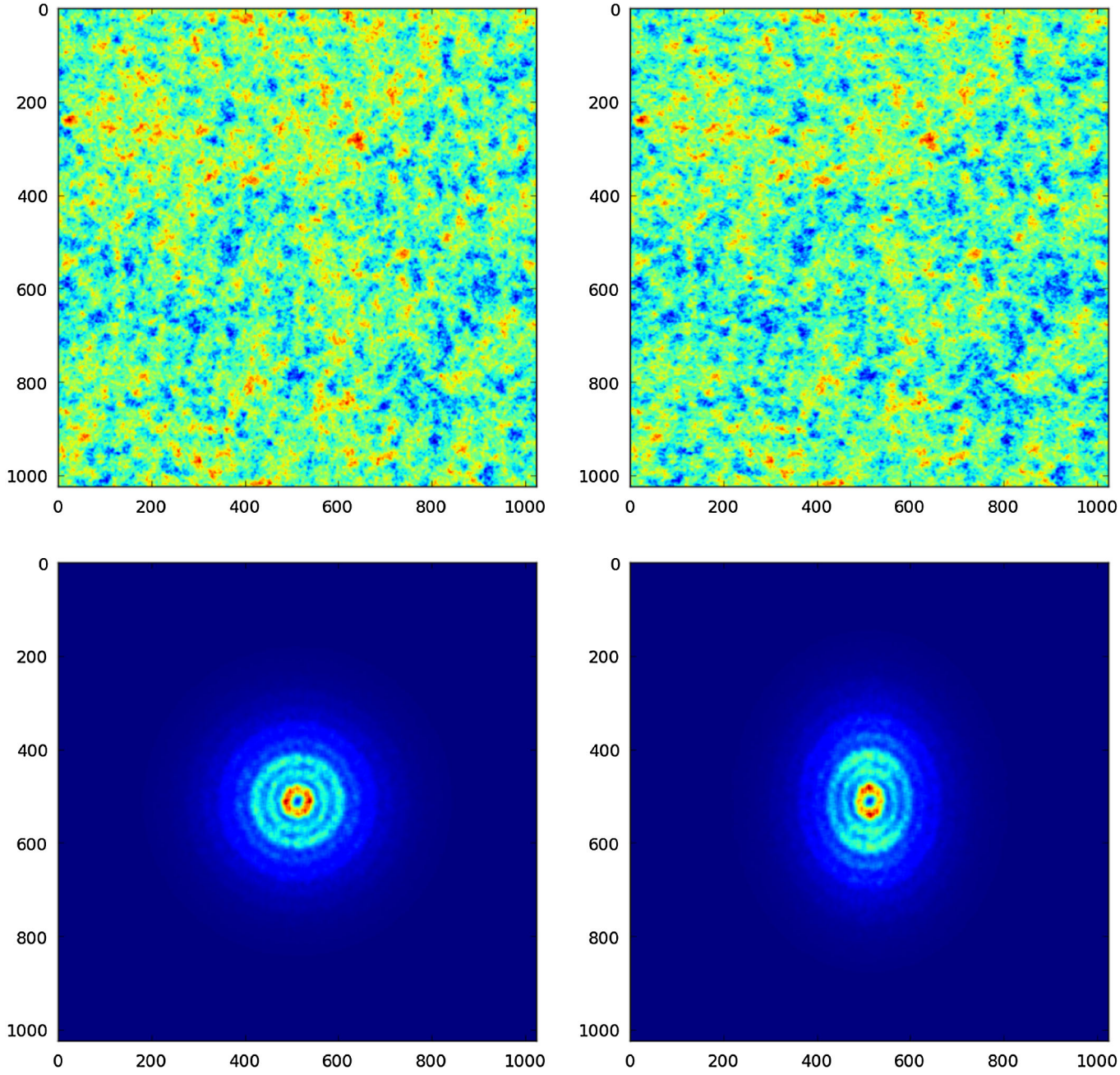

FIG. 1 (color online). *Distortion of power spectrum due to shear.* The plots on the left indicate an unlensed map simulated using the WMAP power spectrum on a torus in angular space (top) and in harmonic space (bottom). The right panels indicate the same simulation but with a 10% pure shear applied. While the maps are almost indistinguishable to the eye in angular space, the shear of the rings (corresponding to acoustic oscillations) in harmonic space is readily apparent.

$$K_{\hat{\gamma}_+,\hat{\gamma}_\times}(\theta) = \frac{1}{N_{\hat{\gamma}_+,\hat{\gamma}_\times}} \int_0^\infty \frac{d\ell}{2\pi} \frac{c(\ell)}{(c(\ell)+n(\ell))^2} \times \left(\frac{d\ln[c(\ell)]}{d\ln[\ell]}\right) J_2(\ell\theta) \tag{19}$$

so that

$$\begin{aligned} \hat{\gamma}_+(\boldsymbol{\theta}) &= T(\boldsymbol{\theta})(K_{\hat{\gamma}_+} \circ T)(\boldsymbol{\theta}), \\ \hat{\gamma}_\times(\boldsymbol{\theta}) &= T(\boldsymbol{\theta})(K_{\hat{\gamma}_\times} \circ T)(\boldsymbol{\theta}), \end{aligned} \tag{20}$$

where

$$\begin{pmatrix} (K_{\hat{\gamma}_+} \circ T)(\boldsymbol{\theta}) \\ (K_{\hat{\gamma}_\times} \circ T)(\boldsymbol{\theta}) \end{pmatrix} = \int d^2\theta' K_{\hat{\gamma}_+,\hat{\gamma}_\times}(|\boldsymbol{\theta}-\boldsymbol{\theta}'|) T(\boldsymbol{\theta}') \times \begin{pmatrix} \cos[2\Theta(\boldsymbol{\theta}-\boldsymbol{\theta}')] \\ \sin[2\Theta(\boldsymbol{\theta}-\boldsymbol{\theta}')] \end{pmatrix} \tag{21}$$

and

$$\tan[2\Theta(\boldsymbol{\theta}-\boldsymbol{\theta}')] = \frac{2(\theta_1-\theta_1')\cdot(\theta_2-\theta_2')}{(\theta_1-\theta_1')^2-(\theta_2-\theta_2')^2}. \tag{22}$$

For the pure shear estimator, there is no need to subtract a bias because $\cos(2\phi)$, $\sin(2\phi)$ make the expectation values vanish for an unlensed sky.

We previously mentioned that the estimators defined in Eqs. (16) and (20) are unbiased and of minimum variance in the $|\ell| \to 0$ limit where ℓ is the wave number of the lensing field. We now turn to the question of how small ℓ has to be for this estimator to be efficient. When $|\ell|$ is no longer small, two things happen: (1) because the above estimators average the lensing field over a finite area, this smoothing causes the components of the lensing field at higher wave numbers to be underestimated; (2) after the scale dependent multiplicative correction has been put in place, the estimator is no longer of minimum variance and thus more noisy than the harmonic quadratic estimator of Hu and Okamoto. We may get an idea of which angular scales contribute most to the statistical weight by considering which ℓ's contribute most to the integrals for $N_{\hat{\kappa}_0}$ and $N_{\hat{\gamma}_+,\hat{\gamma}_\times}$ in Eqs. (13) and (18), respectively. The values of these integrals indicate the $(S/N)^2$ per unit κ_0, γ_+ or $\gamma_\times$, respectively, per unit solid angle.

In order to address this question, we must define a specific CMB experimental configuration, because formally at least these integrals would diverge at large ℓ if there were no instrument noise. In the case of a Gaussian beam, we have

$$n(\ell) = \sigma_p^2 \exp[+\ell^2\theta_{\rm beam}^2] = \sigma_p^2 \exp[+\ell^2/\ell_{\rm beam}^2] \quad (23)$$

where $\theta_{\rm beam}$ is the Gaussian width of the beam, σ_p is the detector noise in a pixel of side $\theta_{\rm beam}$, and the beam cutoff sets in at the multipole $\ell_{\rm beam} = 810(10'/\theta_{\rm fwhm})$, with $\theta_{\rm fwhm}$ the full width at half maximum of the beam. In the simulations in this paper, we shall use the sensitivity and resolution parameters for the Planck experiment (where the 100, 143 and 217 GHz channels have been combined in quadrature) using the values given in the Planck bluebook [29]. The lower two panels of Fig. 2 show the cumulative integrals from, and to, large ℓ after the integrals have been normalized. The relevant quantity that enters into the expression for the cumulative information is the local spectral index, $d\ln C_\ell/d\ln\ell$ (shown in the top right panel of Fig. 2), of the CMB power spectrum (shown in the top left panel of Fig. 2). We observe that the central 80% of the information is concentrated in the range $\ell = 800$–1600. Smaller ℓ contribute almost no information because there are comparatively very few independent multipoles, and moreover

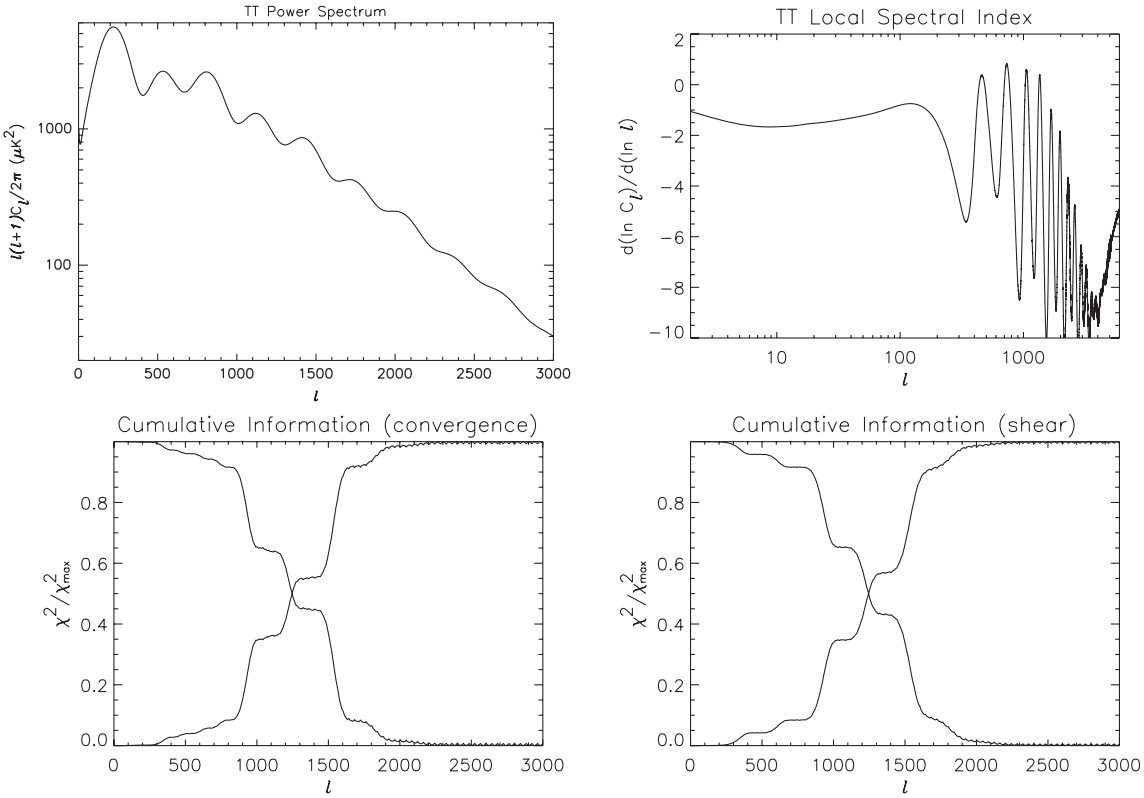

FIG. 2. *Character of the signal.* The top row shows as a function of multipole number ℓ the temperature power spectrum and local spectral index, defined as $d\ln c_\ell/d\ln\ell$, for the standard cosmology (WMAP best-fit model). On the bottom row, the left panel shows the normalized cumulative χ^2 (or equivalently $N_{\hat{\kappa}_0}$ and $N_{\hat{\kappa}_{+,\times}}$) as a function of ℓ integrated both from the left and from the right using the sensitivity and resolution parameters for the Planck experiment (where the 100, 143 and 217 GHz channels have been combined in quadrature) [29].

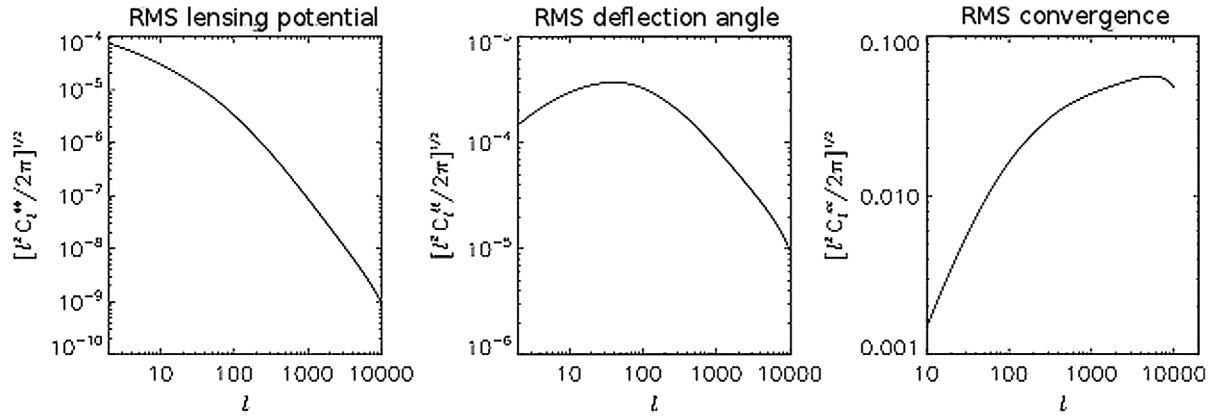

FIG. 3. *Lensing power spectrum.* The lensing field power spectrum is shown represented in several manners. The three panels (from left to right) illustrate the lensing field expressed as a potential, a deflection field, and a convergence/shear field, respectively. Plotted are $[\ell(\ell+1)C_{XX}/(2\pi)]^{1/2}$ where $XX = \Phi\Phi$, $\xi\xi$, $\kappa\kappa$. Here $C_\ell^{\xi\xi} = \ell(\ell+1)C_\ell^{\Phi\Phi}$, and $C_\ell^{\kappa\kappa} = \ell^2(\ell+1)^2 C_\ell^{\Phi\Phi}/4$. Of the three, the last power spectrum is more directly related to the observed distortion.

the angular spectrum in the sky is very nearly scale invariant. At much larger ℓ, instrument noise and beam smearing wash out the usable signal. In the intermediate range a structure of plateaus connected by steep rises can be observed. This structure is a direct result of the Doppler oscillations. Around the crests and troughs the spectrum is almost scale invariant and hence does not contain any information for determining the convergence. In the corresponding plot for the shear, one observes that the plateaus are less pronounced.

The rightmost panel of Fig. 3 shows the shear-convergence power spectrum as a function of multipole number ℓ, and we observe that for $\ell < 100$, the distortion is always less than about 1.5%. This implies that in order to attain an (S/N) of approximately unity it is necessary to consider a region containing at least $O(10^3)$ resolution elements, where a resolution element is a pixel of the map of sufficient size so that the noise and angular resolution of the survey give $S/N \approx 1$. Consequently, there is little point to trying to reconstruct the lensing field over a region not having at least 30 resolution elements on a side. If the distortion from lensing were greater, the situation would be different.

III. REAL SPACE ESTIMATOR WITH TRUNCATED RANGE

In the previous section, we developed simple estimators for the convergence and pure shear components of the gravitational lensing field (see Eqs. (16) and (20)) based on taking the product of a CMB map and a filtered map. We argued that the dominant part of the filters is short-range except for a rapidly falling off tail. This fact suggests that the tail of the filter kernel can be cut off with very little loss. In this section, we investigate the performance of kernels of restricted range in more detail and show how to truncate the filters in an optimal way.

Mathematically, the problem is as follows. We first consider the convergence field estimator, which we require to take the form

$$\hat{\kappa}_0(\boldsymbol{\theta}; \theta_{\max}) = T(\boldsymbol{\theta})(\mathcal{F} \circ T)(\boldsymbol{\theta}) \tag{24}$$

where the kernel $K(\theta; \theta_{\max})$, defining the filter $\mathcal{F}$, vanishes for $\theta \geq \theta_{\max}$. The form of the kernel becomes unique if we add the requirements that the reconstruction be unbiased and of minimum variance in the long-wavelength limit.

To solve this problem, it is convenient to introduce the following inner product in order to reduce the problem to a simple problem in the geometry of Hilbert spaces. Let δc^A and δc^B be small changes with respect to the fiducial power spectrum $c_{\rm fid}$. We define their inner product as

$$\begin{aligned}\langle \delta c^A, \delta c^B \rangle &= \sum_{\ell,m} \frac{1}{2(c_\ell + n_\ell)^2} \delta c^A_{\ell,m} \delta c^B_{\ell,m} \\ &= \mathcal{A} \int \frac{d^2\ell}{(2\pi)^2} \frac{1}{2[c(\ell) + n(\ell)]^2} \delta c^A(\ell) \delta c^B(\ell)\end{aligned} \tag{25}$$

where we give both the spherical and flat sky continuum forms. $\langle \delta c, \delta c \rangle$ represents the $(S/N)^2$ for distinguishing the spectrum $c_{\rm obs} = c_{\rm fid} + \delta c$ from the spectrum $c_{\rm fid}$ in the presence of cosmic variance and instrument noise. Setting $\delta c(\ell)_{\kappa_0=1} \equiv c(\ell)[d\ln c(\ell)/d\ln\ell + 2]$, we may express the estimator $\hat{\kappa}_0$ in Eq. (15) in terms of the above inner product as follows:

$$\begin{aligned}\hat{\kappa}_{0,\rm ideal} &= \frac{\langle \delta c(\ell)_{\kappa_0=1}, \delta c_{\rm obs} \rangle}{\langle \delta c(\ell)_{\kappa_0=1}, \delta c(\ell)_{\kappa_0=1} \rangle} \\ &= \frac{\langle \delta c(\ell)_{\kappa_0=1}, c_{\rm obs} \rangle - \langle \delta c(\ell)_{\kappa_0=1}, c_{\rm fid} \rangle}{\langle \delta c(\ell)_{\kappa_0=1}, \delta c(\ell)_{\kappa_0=1} \rangle}.\end{aligned} \tag{26}$$

We now consider nonideal estimators where $\delta c(\ell)_{\kappa_0=1}$ is replaced by an arbitrary weight vector w, with the ideal

weight vector given by $w_{\rm ideal} = c(\ell)[d\ln c(\ell)/d\ln\ell + 2]$. Using the above inner product, we may define the following unbiased estimator of κ_0

$$\hat{\kappa}_0(w) = \frac{\langle w, \delta c_{\rm obs}\rangle}{\langle w, w_{\rm ideal}\rangle} \tag{27}$$

provided that the denominator does not vanish, with the variance of $\hat{\kappa}_0(w)$ given by $\langle w, w\rangle/\langle w_{\rm ideal}, w\rangle^2$, so that the increase in variance with respect to the ideal estimator is given by the following geometric expression for the secant squared

$$\frac{{\rm Var}(\hat{\kappa}_0(w))}{{\rm Var}(\hat{\kappa}_0(w_{\rm ideal}))} = \frac{\langle w, w\rangle\langle w_{\rm ideal}, w_{\rm ideal}\rangle}{\langle w, w_{\rm ideal}\rangle^2} = \sec^2(\chi). \tag{28}$$

For $\hat{\gamma}_+$ and $\hat{\gamma}_\times$, analogous formulae may be derived straightforwardly.

In real space, according to Eq. (13), the minimum variance full-sky estimator kernel for $\hat{\kappa}_0$ is given by

$$K^{\rm (ideal)}_{\hat{\kappa}_0}(\theta) = \int_0^\infty \ell d\ell J_0(\ell\theta)\frac{1}{2\pi N^{\rm (ideal)}_{\hat{\kappa}_0}}\frac{c(\ell)}{[c(\ell)+n(\ell)]^2} \times\left[\frac{d(\ln[c(\ell)])}{d[\ln(\ell)]}+2\right]. \tag{29}$$

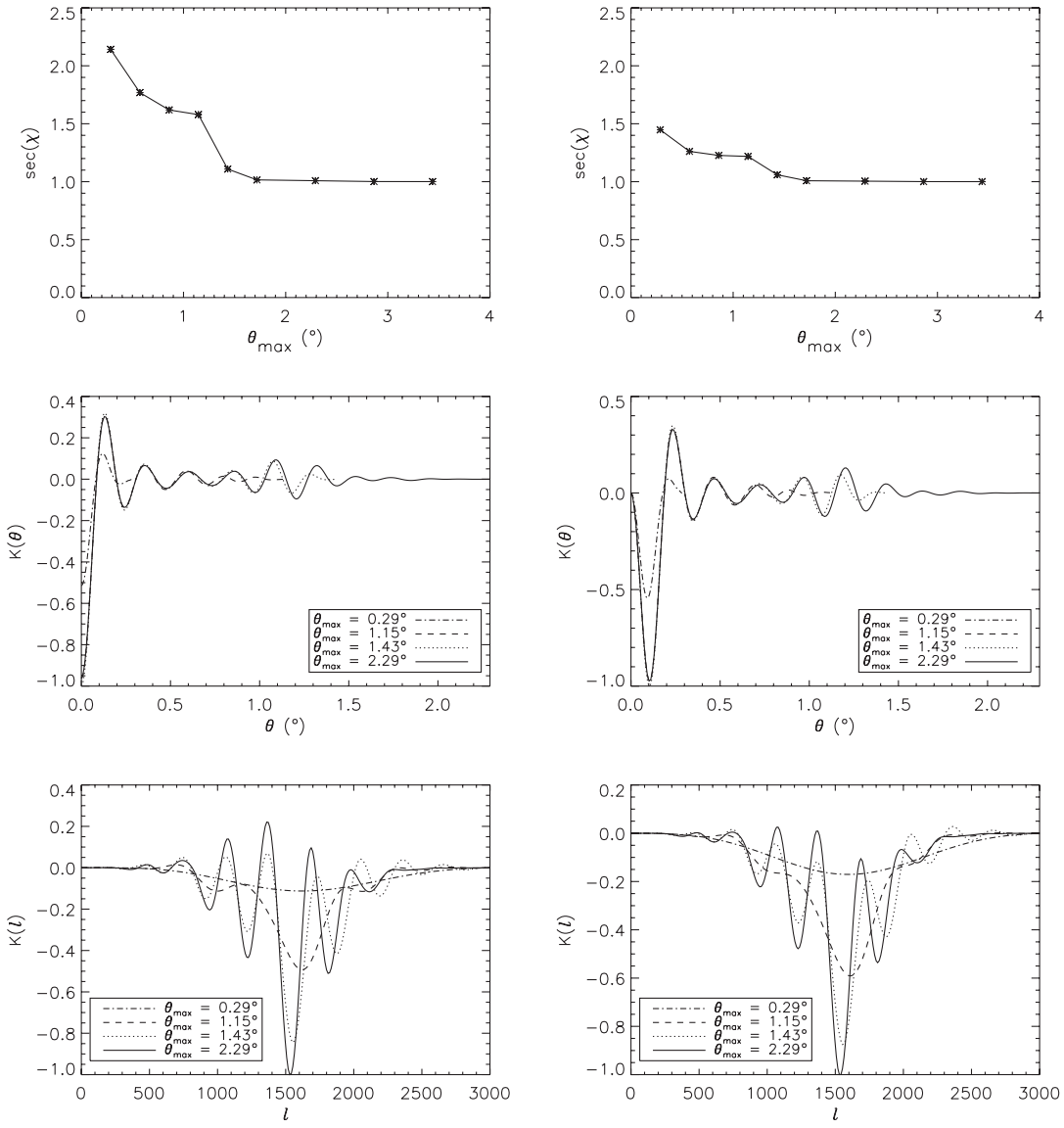

FIG. 4. *Performance of estimator with truncated angular support.* We indicate how limiting the angular support of the filter in our estimator increases the noise. The left panels refer to the convergence filter, while the right panels refer to the shear filter. The top panels indicate how the estimator variance (with the estimator normalized to be unbiased) increases as the angular support (disk radius in degrees) is reduced. The middle and bottom panels indicate the profiles of the optimal truncated estimators in angular and harmonic space, respectively. We assume the experimental noise specifications for the Planck experiment [29] in each of the plots.

This kernel may be inverted using the following inverse Bessel transform

$$\tilde{K}_{\hat{\kappa}_0}(\ell) = \frac{1}{2\pi}\int_0^\infty \theta d\theta J_0(\ell\theta) K_{\hat{\kappa}_0}(\theta). \tag{30}$$

We limit the support of the kernel by requiring that $K_{\hat{\kappa}_0}(\theta)$ be nonzero only for $\theta \leq \theta_{\rm max}$ where $\theta_{\rm max}$ is varied. This is accomplished numerically by expressing $K_{\hat{\kappa}_0}(\theta)$ as a linear combination of cubic spline basis functions spanning the interval $\theta \in [0, \theta_{\rm max}]$ and optimizing for the shape that minimizes the variance calculated according to Eq. (28). Analogous expressions may be obtained for the shear by replacing J_0 with J_2. Figure 4 shows the variance ratio as a function of $\theta_{\rm max}$ for the convergence and shear estimators. The shapes of the kernels of limited angular support are shown in both real and harmonic space. We observe that the increase in variance at small $\theta_{\rm max}$ is more modest for the shear estimator. We also observe that there is a negligible increase in variance of the convergence and shear estimators for $\theta_{\rm max}$ as small as 2° in the case of the Planck experiment. This suggests that it is possible to construct compact versions of the real space lensing estimators that have comparable sensitivity to their harmonic space counterparts.

IV. PERFORMANCE OF REAL SPACE ESTIMATOR

The estimators developed in the previous two sections were derived assuming that the lensing fields vary slowly compared to the small scales at which most of the statistical information exploitable for the lensing reconstruction is located. This implies that in the low-ℓ limit the nontruncated estimator is unbiased and of minimum variance, but as ℓ increases this statement becomes increasingly approximate. In this section, we characterize how the performance degrades with ℓ. Mathematically, the estimators developed above can also be derived as a limiting case of the harmonic estimator first presented by Hu and Okamoto [17,18]. The details of this derivation appear in Appendix A. In a nutshell, the calculation there approximates $c(\ell)$ using $d\ln c(l)/d\ln(l)$ as the leading approximation. Since the scale over which the local effective spectral index varies is approximately $\Delta\ell = 200$, we expect our estimator to break down when the wave number of the lensing field approaches this value. This expectation is borne out in the quantitative comparison that follows, which assumes noise parameters corresponding to a Planck-like survey.

As ℓ increases, the reconstruction is biased by a multiplicative factor equal to unity at $\ell = 0$ and decreasing for larger ℓ. This multiplicative bias arises because the estimator probes the power spectrum over a window of a finite

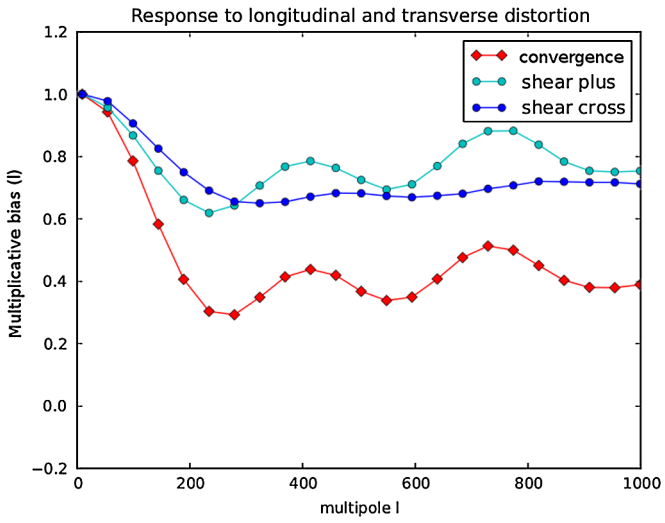

FIG. 5 (color online). *Multiplicative bias of estimators at large lensing wave numbers.* We plot as a function of multipole number the multiplicative biases for the convergence, longitudinal shear, and cross shear reconstructions using the filters described in the text. Noise for the Planck instrument combining the 100 + 143 + 217 GHz channels is assumed using Planck bluebook values and combining channels in quadrature [29].

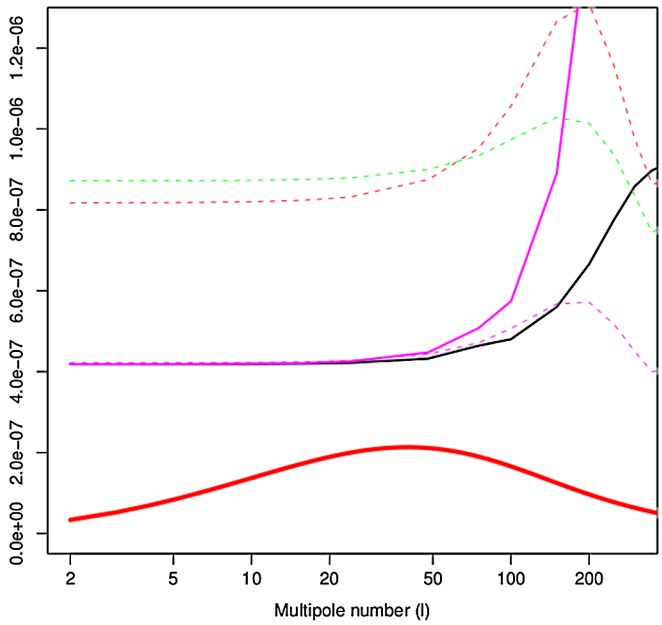

FIG. 6 (color online). *Comparison with quadratic estimator* We plot the noises of the various estimators compared to the expected signal, assuming the experimental specifications for the Planck experiment [29]. The quadratic estimator is indicated in thick black. The convergence and shear estimators are shown in dashed red and green, respectively, and when combined nominally give the dashed magenta curve, but when the imperfect overlap with the expected signal is taken into account, yield the solid magenta curve. The dashed magenta curve would be indicative of the actual noise in the recovered maps, but if the imperfect overlap were corrected to remove the bias at high ℓ the heavy magenta curve would result. For comparison, we show the predicted lensing signal (as computed by CAMB [31] for the WMAP best-fit model [32]) as the heavy red curve.

width in angular space, and consequently smooths the underlying exact lensing field thus reducing its amplitude. We measure the multiplicative bias using simulations, comparing the amplitude of an input plane wave to the amplitude of the recovered signal to derive the loss in power for a range of input wave numbers. The multiplicative bias can also be calculated analytically using the relation between the long-wavelength approximation and the result exact to linear order following the treatment in Appendix A. The multiplicative bias is plotted in Fig. 5 for the convergence, longitudinal shear and transverse shear. We recall that a longitudinal shear is one that can be derived from a potential, and hence is the pure shear predicted from weak lensing, whereas the transverse shear is the B-mode, a longitudinal shear rotated by 45°. The exact shape of the multiplicative bias depends on the filter shape and in turn the experimental noise assumed. We observe that the longitudinal shear estimator experiences less smoothing than the convergence estimator because the form of the ℓ-space filter has less cancellations as can be seen in Fig. 4. This multiplicative bias can be corrected for by appropriate filtering.

At non-negligible ℓ, these estimators also suffer from excess variance, which is shown in Fig. 6. The corresponding expressions for the variance of the different estimators shown in Fig. 6 are presented in Appendix A. At low wave number, the quadratic estimator variance exhibits a flat spectrum, which subsequently diverges at large ℓ. At low ℓ the variance of the quadratic estimator is the same as the quadrature combination of the convergence and longitudinal shear estimators, which indicates that the difference in performance between the estimator developed here and the linearly optimal quadratic estimator is minimal at low ℓ. At higher wave numbers ($\ell \gtrsim 100$), however, the variance of the real space estimator increases rapidly due to lack of overlap with the ideal kernel. There is no simple way to reduce this excess variance other than using another estimator.

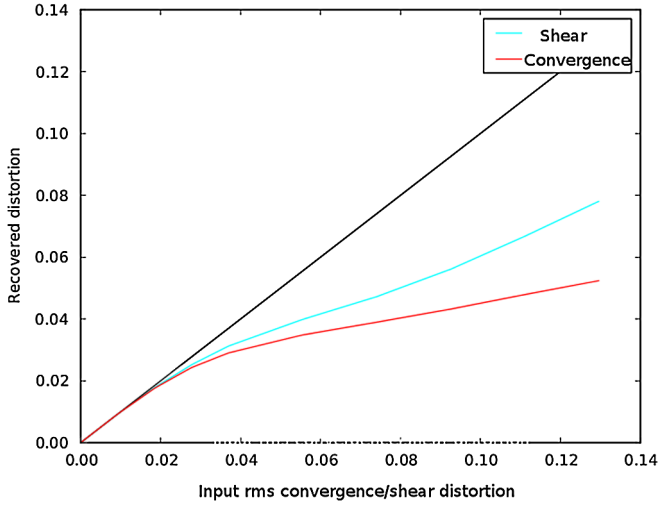

FIG. 7 (color online). *Estimator nonlinearity.* We plot the recovered root-mean-square distortion versus the input root-mean-square distortion in order to characterize the range of linear response for our estimator. The input is a long-wavelength longitudinal deformation, so that the two-dimensional shear and convergence are exactly half the one-dimensional convergence. Exactly the same nonlinearity will plague the quadratic estimator as well, since the two have been demonstrated to be equivalent at low wave numbers.

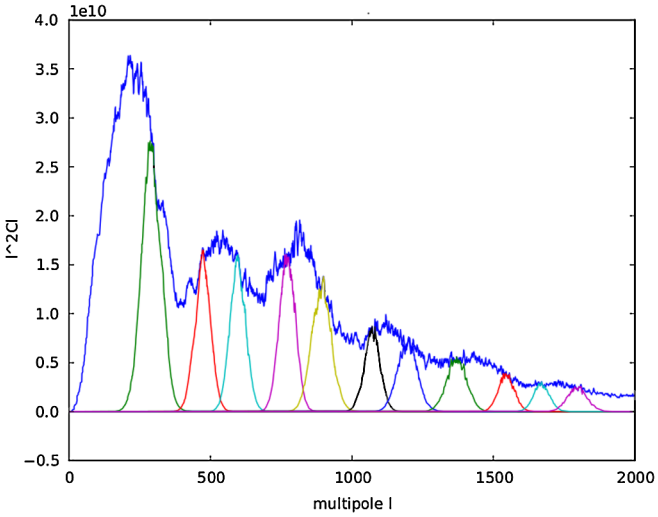

FIG. 8 (color online). *Bandpass filters.* We generate a convergence reconstruction filter by an alternative procedure whereby Gaussian filters are placed at the locations in multipole space where the magnitude of the derivative of $\ell^2 C(\ell)$ is greatest. The widths of the filters are chosen to correspond roughly to the width of the rise and fall of this quantity.

TABLE I. *Performance of individual feature filters.* The first nine entries correspond to Gaussian filters whose centers and widths are indicated and have been placed where the features of the power spectrum change the most in response to a small convergence. The last column expresses the sensitivity of each filter. The next-to-last row shows $(S/N)^2$ resulting when the filters are combined using inverse covariance weighting. This is compared to the ideal filter. The indicated errors result from Monte Carlo noise.

ℓ_{center}	σ_ℓ	$(S/N)^2 \text{deg}^{-2} \cdot \kappa_0^{-2}$
300	50	3.13 ± 0.26
470	40	1.56 ± 0.13
600	40	3.02 ± 0.25
770	40	0.13 ± 0.01
900	50	61.51 ± 5.02
1070	40	23.24 ± 1.90
1200	50	30.66 ± 2.50
1370	50	1.44 ± 0.12
1550	40	42.53 ± 3.47
Optimal linear combination		167.22 ± 13.65
Ideal filter		140.50 ± 11.47

Another possible source of error arises from nonlinearity, which sets in when the local power spectrum is distorted so much that the first derivative approximation is no longer valid. This problem is inherent to all quadratic estimators, and the multiplicative error factor is shown in Fig. 7 as a function of the amplitude of the distortion. We observe that the linear response breaks down when the root-mean-square convergence or pure shear is around 2–3%. Ignoring higher order terms in the deflection angle expansion thus gives

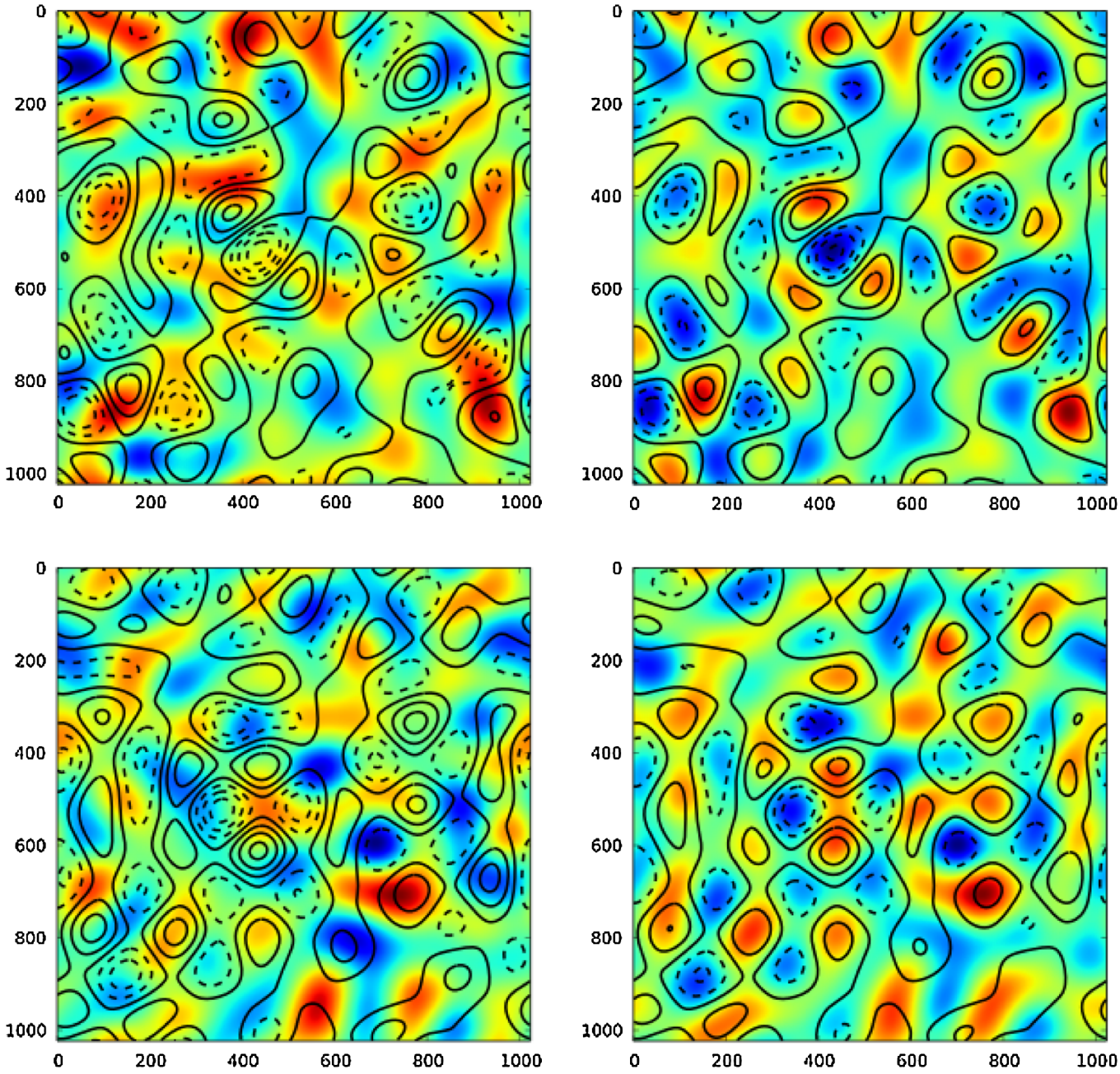

FIG. 9 (color online). *Simulations of lensing reconstruction.* We simulate CMB maps on a $40° \times 40°$ flat region of the sky assuming 7 yr WMAP best-fit cosmological parameters [32] and the lensing predicted within the framework of this model. In the top row the convergence is shown for practically no lensing, actually one twentieth the predicted signal (left) and the predicted signal boosted by a factor of five (right). The contours show the predicted signal and the pseudocolor image shows the recovered signal. Both maps are normalized so as to highlight the degree of correlation manifested as the coincidence of the contours and lines of constant color. The bottom row shows the same plots but with one of the two shear components. Whereas on the left there is no visible correlation, on the right the agreement is very good, although some noise is still visible. The maps of the underlying and reconstructed convergence and shear have been filtered using a filter centered at $\ell = 20$ of width $\Delta\ell/\ell = 0.3$.

rise to a bias in these estimators which must be corrected [24,30].

V. ESTIMATORS TARGETING PARTICULAR FEATURES

In this section, we digress slightly showing how lensing can be reconstructed focusing on particular features of the CMB temperature spectrum. We concentrate on the convergence field reconstruction. Eqs. (12) and (13) indicate that those values of ℓ for which the local spectral index is scale-invariant ($d\ln c(l)/d\ln(\ell) \approx -2$) contribute no useful information for the lensing reconstruction. The filter implied by Eq. (12) weights values of ℓ for which $\ell^2 c(\ell)$ rises with the opposite sign compared to those values where $\ell^2 c(\ell)$ falls.

This suggests that one could develop a series of estimators of κ_0 filtering around the various rises and falls in the power spectrum $\ell^2 c(\ell)$, as indicated in Fig. 8. Table I indicates the noise levels associated with each of the features in the spectrum. It is intriguing to notice that when these partial estimators are combined according to inverse variance weighting, the total noise of the reconstruction is the same as the ideal estimator in Eq. (12) to within the error of our Monte Carlo simulations. Ideas along these lines could prove useful in diagnosing systematic errors in the lensing reconstruction.

VI. SIMULATIONS AND CONCLUDING REMARKS

We have demonstrated how to reconstruct in real space using a filter of compact support the weak gravitational lensing field, here represented as three fields, a convergence field $\kappa_0(\boldsymbol{\theta})$ and the two components of the pure shear distortion field $\gamma_+(\boldsymbol{\theta})$ and $\gamma_\times(\boldsymbol{\theta})$. To demonstrate that the estimator works as claimed, we generated lensed and unlensed CMB maps on a 40° x 40° square region assuming the 7 yr WMAP best-fit cosmological model and the associated lensing power spectrum. The results are shown in Fig. 9, where the expected lensing signal has been enhanced by a factor of five in order to make the correlations between the recovered and input lensing apparent to the eye without a detailed statistical analysis. The top row shows the recovered convergence map with no lensing (left) and lensing (right). The bottom row shows the same for one of the two pure shear components. It is clear that there is no visible correlation between the predicted and recovered signals in the absence of lensing, whereas the degree of correlation in the lensing case is very good, although some noise is still visible.

Except for an integration constant and two translational and one rotational zero modes, the weak lensing may alternatively, and equivalently, be described by either (1) a gravitational lensing potential $\Phi(\boldsymbol{\theta})$, (2) a displacement field $\boldsymbol{\xi}(\boldsymbol{\theta})$, or (3) the convergence field $\kappa_0(\boldsymbol{\theta})$ and the two components of the pure shear distortion field $\gamma_+(\boldsymbol{\theta})$ and $\gamma_\times(\boldsymbol{\theta})$. In this paper we argue that for the purpose of reconstruction the representation (3) is advantageous because this is the representation for which the lensing field bears a local relation to the real space CMB maps. This locality comes at a price because the three components are not independent and subject to nonlocal consistency conditions, which may be exploited to improve the reconstruction. Locality allows different regions of the sky to be analyzed independently in a natural way, quite unlike the quadratic reconstruction in harmonic space, where the entire sky must be analyzed simultaneously. This approach and variations thereof hold promise for dealing with partial sky coverage and excised point sources. For the filters developed in this paper there is very little loss of information for the lensing field at low wave numbers. However at larger wave numbers the lensing signal is attenuated according to a wave number dependent multiplicative bias, which can be deconvolved by applying a correction filter.

ACKNOWLEDGMENTS

M. B. and K. M. acknowledge support from a joint CNRS/NRF travel grant. The work of M. B., C. S. C. and M. R. was supported in part by the Projet Blanc VIMS-PLANCK of the Agence Nationale de la Recherche. K. M. is supported by the South African National Research Foundation (NRF). C. S. C. was supported by the South African NRF and is currently supported by Fundação para a Ciência e a Tecnologia, Grant No. SFRH/BPD/65993/2009.

APPENDIX A: COMPARISON WITH THE HU AND OKAMOTO QUADRATIC ESTIMATOR

We provide here the details showing that the estimator defined in Eq. (1) is a limiting case of the quadratic harmonic estimator of Hu and Okamoto. In angular space, the change in the temperature map due to lensing (valid to linear order) is given by

$$\delta T(\boldsymbol{\theta}) = \nabla\Phi(\boldsymbol{\theta}) \cdot \nabla T(\boldsymbol{\theta}), \tag{A1}$$

which in harmonic space translates into

$$\delta T(\boldsymbol{\ell}) = \int \frac{d^2\ell'}{(2\pi)^2} (-\boldsymbol{\ell}') \cdot (\boldsymbol{\ell} - \boldsymbol{\ell}') \Phi(\boldsymbol{\ell}') T(\boldsymbol{\ell} - \boldsymbol{\ell}') \tag{A2}$$

where we define $\langle T(\boldsymbol{\ell}) T(\boldsymbol{\ell}')\rangle = (2\pi)^2 \delta^2(\boldsymbol{\ell} + \boldsymbol{\ell}') c(\ell)$. Since $T_{\rm sky} = T + \delta T$, it follows that to leading (linear) order

$$\begin{aligned}\left\langle T_{\rm sky}\left(\frac{\boldsymbol{\ell}'}{2} + \boldsymbol{\ell}\right) T_{\rm sky}\left(\frac{\boldsymbol{\ell}'}{2} - \boldsymbol{\ell}\right)\right\rangle &= \Phi(\boldsymbol{\ell}') \times \left[\left(\frac{\boldsymbol{\ell}'}{2} - \boldsymbol{\ell}\right) \cdot \boldsymbol{\ell}' c\left(\left|\boldsymbol{\ell} - \frac{\boldsymbol{\ell}'}{2}\right|\right)\right. \\ &\left. + \left(\frac{\boldsymbol{\ell}'}{2} + \boldsymbol{\ell}\right) \cdot \boldsymbol{\ell}' c\left(\left|\boldsymbol{\ell} + \frac{\boldsymbol{\ell}'}{2}\right|\right)\right].\end{aligned} \tag{A3}$$

It follows that

$$\hat{\Phi}(\ell') = N^{-1}\sum_{\ell} W(\ell';\ell) T_{\rm sky}\left(\frac{\ell'}{2}+\ell\right) T_{\rm sky}\left(\frac{\ell'}{2}-\ell\right) \quad \text{(A4)}$$

is the minimum variance unbiased estimator for the Fourier coefficient $\Phi(\ell')$ where

$$W(\ell';\ell) = \frac{[(\frac{\ell'}{2}-\ell)\cdot\ell' c(|\ell-\frac{\ell'}{2}|) + (\frac{\ell'}{2}+\ell)\cdot\ell' c(|\ell+\frac{\ell'}{2}|)]}{[c(\ell-\frac{\ell'}{2})+n(\ell-\frac{\ell'}{2})][c(\ell+\frac{\ell'}{2})+n(\ell+\frac{\ell'}{2})]} \quad \text{(A5)}$$

and

$$N = \sum_{\ell} \frac{[(\frac{\ell'}{2}-\ell)\cdot\ell' c(|\ell-\frac{\ell'}{2}|) + (\frac{\ell'}{2}+\ell)\cdot\ell' c(|\ell+\frac{\ell'}{2}|)]^2}{[c(\ell-\frac{\ell'}{2})+n(\ell-\frac{\ell'}{2})][c(\ell+\frac{\ell'}{2})+n(\ell+\frac{\ell'}{2})]}. \quad \text{(A6)}$$

We may approximate the quantity in the square brackets in Eq. (A3) to linear order assuming $|\ell'| \ll |\ell|$ to obtain

$$\begin{aligned}
&\left(\frac{\ell'}{2}-\ell\right)\cdot\ell' c\left(\left|\ell-\frac{\ell'}{2}\right|\right) + \left(\frac{\ell'}{2}+\ell\right)\cdot\ell' c\left(\left|\ell+\frac{\ell'}{2}\right|\right) \\
&\quad = \ell'^2 c(\ell) + (\ell\cdot\ell')^2 \frac{1}{\ell}\frac{\partial c(\ell)}{\partial \ell} \\
&\quad = \frac{1}{2}\frac{\ell'^2}{\ell^2}\frac{\partial[\ell^2 c(\ell)]}{\partial \ln[\ell]} + \left(\frac{(\ell\cdot\ell')^2 - \frac{1}{2}\ell'^2\ell^2}{\ell^2}\right)\frac{\partial[c(\ell)]}{\partial \ln[\ell]} \\
&\quad = +\frac{1}{2}\ell'^2\left\{\frac{1}{\ell^2}\frac{\partial[\ell^2 c(\ell)]}{\partial \ln[\ell]} + \cos[2\Theta]\frac{\partial[c(\ell)]}{\partial \ln[\ell]}\right\} \qquad \text{(A7)}
\end{aligned}$$

where Θ is the angle between ℓ and ℓ'. Approximating the numerator of (A5) as (A7) and the denominator of (A5) as $[c(\ell)+n(\ell)]^2$, we obtain

$$\begin{aligned}
\widehat{\nabla^2\Phi}(\ell') = \frac{1}{2}\frac{1}{N_{\widehat{\nabla^2\Phi}}}\int \frac{d^2\ell}{(2\pi)^2}\frac{-[c(\ell)]}{[c(\ell)+n(\ell)]^2} \\
\times\left[\frac{\partial(\ln[\ell^2 c(\ell)])}{\partial[\ln(\ell)]} + \cos[2\Theta(\ell,\ell')]\right. \\
\left.\times\frac{\partial(\ln[c(\ell)])}{\partial[\ln(\ell)]}\right] T_{\rm sky}\left(\frac{\ell'}{2}-\ell\right) T_{\rm sky}\left(\frac{\ell'}{2}+\ell\right) \qquad \text{(A8)}
\end{aligned}$$

where

$$\begin{aligned}
N_{\widehat{\nabla^2\Phi}}(\ell') = \frac{1}{4}\int \frac{d^2\ell}{(2\pi)^2}\frac{[c(\ell)]^2}{[c(\ell)+n(\ell)]^2} \\
\times\left[\frac{\partial(\ln[\ell^2 c(\ell)])}{\partial[\ln(\ell)]} + \cos[2\Theta(\ell,\ell')]\frac{\partial(\ln[c(\ell)])}{\partial[\ln(\ell)]}\right]^2. \qquad \text{(A9)}
\end{aligned}$$

Because the cross terms cancel under the integral, we may rewrite the above normalization factor as

$$\begin{aligned}
&\frac{1}{4}\mathcal{A}\int\frac{d^2\ell}{(2\pi)^2}\frac{[c(\ell)]^2}{[c(\ell)+n(\ell)]^2}\left[\frac{\partial(\ln[\ell^2 c(\ell)])}{\partial[\ln(\ell)]}\right]^2 \\
&\quad + \frac{1}{4}\mathcal{A}\int\frac{d^2\ell}{(2\pi)^2}\frac{[c(\ell)]^2}{[c(\ell)+n(\ell)]^2} \\
&\quad \times\left[\cos[2\Theta(\ell,\ell')]\frac{\partial(\ln[c(\ell)])}{\partial[\ln(\ell)]}\right]^2 \qquad \text{(A10)}
\end{aligned}$$

which is simply equal to the sum of $N_{\hat{\kappa}_0}$ and $N_{\hat{\gamma}_+}$ previously defined in Eqs. (12) and (17) in Sect. II. We obtain the following relation between the Hu and Okamoto estimator and ours valid in the long-wavelength limit:

$$\begin{aligned}
\widehat{\nabla^2\Phi}(\ell') = \frac{N_{\hat{\kappa}_0}(\ell')}{N_{\hat{\kappa}_0}(\ell')+N_{\hat{\gamma}_+}(\ell')}2\hat{\kappa}_0(\ell') \\
+\frac{N_{\hat{\gamma}_+}(\ell')}{N_{\hat{\kappa}_0}(\ell')+N_{\hat{\gamma}_+}(\ell')}2\hat{\gamma}_+(\ell'), \qquad \text{(A11)}
\end{aligned}$$

which is simply the inverse variance weighted linear combination of the convergence and pure shear longitudinal component with respect to ℓ' from Sec. II. The other component of the shear is forbidden for weak lensing.

[1] A. Blanchard and J. Schneider, A&A International **184**, 1 (1987).

[2] S Cole and G Eftstathiou, Mon. Not. R. Astron. Soc. **239**, 195 (1989).

[3] K. Tomita and K. Watanabe, Prog. Theor. Phys. **82**, 563 (1989).

[4] F. Bernardeau, A&A International **324**, 15 (1997); **338**, 767 (1998).

[5] L. Van Waerbeke, F. Bernardeau, and K. Benabed, Astrophys. J. **540**, 14 (2000).
[6] U. Seljak, Astrophys. J. **463**, 1 (1996).
[7] U Seljak and M Zaldarriaga, Phys. Rev. Lett. **78**, 2054 (1997); M. Zaldarriaga and U Seljak, Phys. Rev. D **58**, 023003 (1998).
[8] K. Benabed, F. Bernardeau, and L. van Waerbeke, Phys. Rev. D **63**, 043501 (2001).
[9] U. Seljak and C. M. Hirata, Phys. Rev. D **69**, 043005 (2004).
[10] M. Zaldarriaga, Phys. Rev. D **62**, 063510 (2000).
[11] A. Cooray, Phys. Rev. D **65**, 063512 (2002).
[12] A. Cooray and M. Kesden, New Astron. Rev. **8**, 231 (2003).
[13] M. Kesden, A. Cooray, and M. Kamionkowski, Phys. Rev. D **66**, 083007 (2002).
[14] W. Hu, Phys. Rev. D **62**, 043007 (2000).
[15] W. Hu, Astrophys. J. **557**, L79 (2001).
[16] W. Hu, Phys. Rev. D **64**, 083005 (2001).
[17] W. Hu and T. Okamoto, Astrophys. J. **574**, 566 (2002).
[18] T. Okamoto and W. Hu, Phys. Rev. D **67**, 083002 (2003).
[19] A. Challinor and A. Lewis, Phys. Rev. D **71**, 103010 (2005); Phys. Rep. **429**, 1 (2006).
[20] J. Lesgourgues, L. Perotto, S. Pastor, and M. Piat, Phys. Rev. D **73**, 045021 (2006).
[21] S. Das and P. Bode, arXiv:astro-ph/07113793.
[22] K. M. Smith, O. Zahn, and O. Dore, Phys. Rev. D **76**, 043510 (2007).
[23] D. Hanson, G. Rocha, and K. Gorski, Mon. Not. R. Astron. Soc. **400**, 2169 (2009).
[24] C. M. Hirata and U. Seljak, Phys. Rev. D **67**, 043001 (2003).
[25] C. M. Hirata and U. Seljak, Phys. Rev. D **68**, 083002 (2003).
[26] N. J. Miller, M. Shimon, and B. G. Keating, Phys. Rev. D **79**, 063008 (2009).
[27] L. Perotto, J. Bobin, S. Plaszczynski, J.-L. Starck, and A. Lavabre, arXiv:astro-ph/0903.1308.
[28] C. S. Carvalho and K. Moodley, Phys. Rev. D **81**, 123010 (2010).
[29] The Planck Collaboration, ESA-SCI 1, 2005.
[30] M. Kesden, A. Cooray, and M. Kamionkowski, Phys. Rev. D **67**, 123507 (2003).
[31] A. Lewis, A. Challinor, and A. Lasenby, Astrophys. J. **538**, 473 (2000).
[32] D. Larson *et al.*, Astrophys. J. Suppl. Ser. **192**, 16 (2011).